Author Manuscript

Study of Histotripsy with Subsequent Heating on *in vitro* VX2 Cancer Cells

Qizheng Dai[a], Lisa X. Xu[a], Aili Zhang[a,*], J. Brian Fowlkes[b,*]

[a]*School of Biomedical Engineering, Shanghai Jiao Tong University, 400 Med-X Research Institute, No.1954 Huashan Rd, Shanghai, 200030, China*
[b]*Department of Radiology, University of Michigan Health System, 6428B, Medical Science Building I, 1301 Catherine Street, Ann Arbor, MI 48109, USA*

Abstract

Objective – Focused ultrasound has emerged as a precise and minimally-invasive modality for effective cancer treatment. In this study, we propose a novel method that integrates the mechanical effects of focused ultrasound, known as histotripsy, with heating to enhance both the immediate and sustained cytotoxic effects on cancer cells.

Methods – Our investigation focused on VX2 cancer cells in suspension, examining five experimental groups: blank control, negative control, heating alone, histotripsy alone, and histotripsy with subsequent heating. B-mode ultrasound imaging was utilized to visualize cavitation bubble cloud formation and its motion during histotripsy. The suspension was contained in individually sealed compartments obtained from bubble wrap (referred to as bubble wrap compartments) embedded within the agarose phantom. Resid-

*Address correspondence to: Aili Zhang, School of Biomedical Engineering, Shanghai Jiao Tong University, No.1954 Huashan Rd, Xuhui District, Shanghai, China, E-mail: zhangaili@sjtu.edu.cn; J. Brian Fowlkes, Department of Radiology, University of Michigan Health System, 6428B, Medical Science Building I, 1301 Catherine Street, Ann Arbor, MI 48109, USA, E-mail: fowlkes@umich.edu

This is the author manuscript accepted for publication and has undergone full peer review but has not been through the copyediting, typesetting, pagination and proofreading process, which may lead to differences between this version and the Version of Record. Please cite this article as doi: 10.1002/jum.16649

This article is protected by copyright. All rights reserved.

Author Manuscript

ual living cells were examined immediately after treatment and cultured for 96 hours to analyze the growth patterns. Additionally, CFDA SE staining was employed to assess cell proliferation. Furthermore, both intracellular and extracellular heat shock protein 70 (HSP70) levels were measured to investigate the potential initiation of an immune response.

Results – The combination of histotripsy and subsequent heating significantly reduced the normalized concentration of living cells immediately after treatment. It also decreased the proliferation rate of residual cells compared to the other experimental groups. Histotripsy with subsequent heating also increased the generation and release of HSP70, which might potentially enhance an innate anti-tumor immune response *in vivo*.

Conclusion – Histotripsy and subsequent heating improved immediate lethal impact on VX2 cancer cells and curtailed the proliferation of residual cancer cells in suspension. This study presents a promising strategy for cancer therapy in the future.

Keywords: Histotripsy, Thermal Therapy, Combination Therapy, Ultrasound Therapy Phantom, Cell–Bubble Interactions, HSP70

Author Manuscript

Introduction

Focused ultrasound can treat tumors in a minimally invasive manner under imaging guidance [1] through various methods based on how ultrasound energy interacts with tissues. For example, high intensity focused ultrasound (HIFU) is typically used to induce thermal effects, while histotripsy relies on mechanical effects. HIFU employs focused acoustic waves (0.5 MHz to 10 MHz) [2] to induce coagulative necrosis by raising temperatures above 55℃ at the focal point [3]. In contrast, histotripsy leverages the cavitation effect of HIFU in a mechanical manner, involving the generation, oscillation, and collapse of bubbles [4]. In shock-scattering histotripsy, an individual nucleus initially forms near the focal point in the ultrasound field. These bubbles scatter the incident shock waves to form a dense bubble cloud [5]. The subsequent collapse of the bubble cloud imparts intense localized strain, fracturing cells into acellular debris [6, 7], and resulting in target disintegration and liquefaction [8]. Histotripsy minimizes deposited thermal energy by applying repeated short-duration pulses with low duty cycles instead of continuous waves [9, 10, 11, 12]. Additionally, the peak acoustic intensity in histotripsy could be up to 5 times higher than in thermal ablation [10, 13]. The tissue-specific susceptibilities to histotripsy allow for selective damage [14]. Because of their high mechanical strength, larger blood vessels and bile ducts remain intact within the completely fractionated targeted tissues [7]. Furthermore, histotripsy is less susceptible to heat sink effects or perfusion.

Histotripsy has been successfully investigated across various tissues, including osteosarcoma specimens [15], uterine fibroid specimens [16], and liver tumor specimens embedded in gelatin phantoms [17]. Histopathological eval-

Author Manuscript

uations of these specimens have consistently demonstrated effective cell ablation in treated areas. Further in vivo experiments in animals have explored the efficacy of histotripsy on subcutaneous tumors [18], cholangiocarcinoma [19], and prostate tumors [20]. Beyond local ablation, several studies have reported abscopal effects following histotripsy. Qu et al. utilized histotripsy on subcutaneous murine melanoma tumors in C57BL/6 mice model and found abscopal immune responses as inhibited growth of pulmonary metastases [21]. In a clinical case, a patient with colorectal cancer and hepatic metastases underwent histotripsy on one liver lesion, ending up with size reduction in both treated lesion and untreated lesions in other lobes of the liver [22].

Expanding the study to the molecular level, Pahk et al. [23] exposed MDA-MB-231 breast cancer cells to boiling histotripsy (BH) in liquid media. Their observations indicated a gradual increase in danger signals (calreticulin (CRT), heat shock proteins (HSPs), high mobility-group box 1 (HMGB-1)), pro-inflammatory cytokines (interferon and interleukin family), and chemokines. Co-incubation of monocytes with the supernatant led to the polarization of M1 macrophages, resulting in cell death through TNF-induced necrosis. In C57BL/6 mice bearing B16GP33 tumors, Qu et al. [21] observed an increase in neutrophils, NK cells, dendritic cells, macrophages, helper T cells, and B cells, and a decrease in regulatory T cells after histotripsy. Additionally, van den Bijgaart et al. [24] found that histotripsy induced unique fragmented profiles of RNA, DNA, and proteins, and decreased immunosuppressive factors such as $TGF-\beta$ and $IL-10$ in tumor debris in C57BL/6 mice bearing EG.7-OVA lymphoma, compared to thermal HIFU. It is believed that histotripsy might lead to the release of non-thermally dam-

Author Manuscript

aged antigens, thus potentially inducing a stronger antigen-specific immune response [25].

Additionally, heating has profound bioeffects, including cell membrane collapse, protein denaturation, mitochondrial dysfunction, and halted enzyme function [26]. Immune responses have been observed in various heating treatments, including photothermotherapy [27], radiofrequency heating [28], microwave heating [29], interstitial laser hyperthermia [30], and whole-body hyperthermia (WBH) [31, 32, 33]. A treatment which utilized freezing to pretreat tumors before heating was found to significantly boost the anti-tumor immune response through increased release of antigens and danger signals, which subsequently activated $CD4^+$ T cells [34, 35]. Compared to freezing, histotripsy created larger treatment zones and resulted in similar changes in serum creatinine [36]. With the motivation of further enhancing the therapeutic outcomes of histotripsy, we are particularly interested in the combination of histotripsy with subsequent heating at 50℃, as research on this combination remains limited [37].

Here we introduced a cancer therapy that combines histotripsy with subsequent heating. The primary hypothesis was that histotripsy could promptly and mechanically damage cancer cells, while the subsequent heating further suppressed the proliferation of residual cancer cells (Fig. 1(a)). To investigate the cellular mechanisms of histotripsy with subsequent heating, we have embedded bubble wrap compartments into the agarose phantom as containers for liquid media. The residual cancer cells following various treatments were collected, re-cultured, and examined. Subsequently, the suspension was analyzed for both intracellular and extracellular HSP70 to gain insights into

Author Manuscript

the therapeutic effects.

Materials and Methods

Experimental procedure

The cancer cell experiments were conducted with five groups: blank control, negative control, heating alone, histotripsy alone, and histotripsy with subsequent heating (Fig. 1(b)). The blank control group underwent standard culture and collection procedures, while distinct treatments were applied to the remaining four groups.

Cell Culture

The VX2 cancer cell line was procured from the National Cancer Institute Division of Cancer Treatment Diagnosis and Treatment Tumor/Cell Line Repository (NCI-DTP) [38]. Cells were cultured in DMEM media (Hyclone, Logan, UT, USA), supplemented with 10% FBS (Gemini Bio-Products), and 100 $units/mL$ penicillin & 100 $\mu g/mL$ streptomycin (Shanghai Sangon, Shanghai, China), and maintained at 37℃ in a humidified 5% CO_2 incubator.

Phantom preparation

A three-layer phantom was developed following the method inspired by Maxwell et al [39]. BioWest regular agarose G-10 powder was dissolved in physiological saline ($0.7g/100mL$ at 25℃) and heated in a Büchner flask until transparent. Simultaneously, a circulating water vacuum pump (SHZ-D(III), Shanghai Exceed Instruments Co., Ltd, China) degassed the mixture, which was confirmed using a portable dissolved oxygen meter (JBP-607A, Shanghai

Author Manuscript

Measuretech Instrument Co., Ltd, China). Customized acrylic containers (120 $mm\times$ 50 $mm\times$ 50 mm) were prepared and initially filled with 200 mL of the mixture. Before full solidification, bubble wrap compartments (10 mm in diameter, 6 mm in height, catalog number 100045139599, Shanghai Yuanmai Trading Co., Ltd, China) were gently placed in two rows with a 5 mm interval, adhering to the solidified mixture through surface tension. The compartment size was selected from commercially available bubble wraps with verified ability of culturing and storing liquid biological samples [40]. The cavitation bubble cloud could be generated throughout the cell suspension contained in the bubble wrap compartments based on the ultrasound imaging and sufficient cells could be harvested for assessment. After refrigerating at 4℃ for complete solidification, additional mixture was poured over the bubble wrap compartments to form a second layer. The solidification process was repeated, and the remaining mixture was added to form the top layer. The phantom was then stored at 4℃ and covered with parafilm to prevent dehydration (Fig. 2(a)). The acoustic and mechanical properties of the agarose gel phantom have been previously measured. The shear modulus density, surface tension, and density were 18.6 kPa, 0.023 N/m, and 1070 kg/m^3 [41]. The speed of sound and attenuation were 1526.19 m/s and 0.1118 dB/cm at 1 MHz [42].

Injection of cell suspension in phantom

VX2 cancer cells were harvested and suspended at a concentration of 2,000,000 cells/mL in DMEM media with 10% FBS, 100 $units/mL$ penicillin, and 100 $\mu g/mL$ streptomycin. Two 22-gauge needles were inserted into each bubble wrap compartment simultaneously. The cancer cell suspension was

Author Manuscript

gently injected to fill the bubble wrap compartments using a syringe attached to one of the needles (Fig. 2(b)), with the other needle facilitating the air release to maintain pressure balance.

B-mode ultrasound imaging

B-mode ultrasound (US) images were captured before and during histotripsy using either a LOGIQ e ultrasound scanner (GE HealthCare, Austria) equipped with a linear probe (12L-RS, GE HealthCare, Austria) or an X3PRO ultrasound scanner (SonoScape Medical Corp, Guangdong, China) equipped with a linear probe (L741, Sonoscape Medical Corp, Guangdong, China). The imaging probe was positioned, as shown in Fig. 3 in a longitudinal view along the propagation direction of the therapy transducer to visualize histotripsy activity in a given bubble wrap compartment. The X axis was defined as the ultrasound propagation direction with the Z axis parallel to the direction of gravity.

Histotripsy generation

For therapy, a single-element transducer (H-108, Sonic Concepts, Inc., Bothell, USA) with a 60 *mm* active diameter and 39.4 *mm* focal depth operating at a center frequency of 2.7 MHz was utilized. The -3dB bandwidth ranged from 1.74 MHz to 3.5 MHz. Manufacturer-supplied testing results indicated an impedance of 46.8 Ω at the center frequency and a phase of 6.6°, with expected focal dimensions of 0.51 *mm* in width and 3.28 *mm* in length (at -6dB points) in degassed water. The input voltage to the transducer was monitored using a digital oscilloscope (MSO-X 2022A, Agilent Technologies, Inc., Santa Clara, CA). An A/B class amplifier (AG1006, T&C

Author Manuscript

Power Conversion, Rochester, NY) drove the transducer, and the amplifier's input came from a function/arbitrary waveform generator (33210A, Agilent Technologies, Inc., Santa Clara, CA). A 2.7 MHz sine wave with a pulse repetition frequency (PRF) of 100 Hz and a pulse width of 200 μs was generated. A PRF of 100 Hz was used in our study because PRF in the range of 1 to 1000 Hz has been commonly used for shock-scattering histotripsy [43]. Additionally, a pulse width of 200 μs was selected because histotripsy produced by hundred-microsecond-long focused ultrasound pulses could rapidly generate mechanically homogenized lesions in phantoms and kidney tissue [44]. Post-amplification, the peak negative voltage to the transducer reached 145V. The instantaneous peak electrical power was $\sim$450 W, calculated using Ohm's law. With a power conversion efficiency of 70% tested by the manufacturer, the peak acoustical power output at the surface of transducer is estimated to be 314 W. The pressure calculations were conducted using a method inspired by Xin et al [45]. The electric power was extrapolated from measurements at lower voltages (20 to 60 V). Subsequently, the focal pressure was calculated using the modified KZK equation [46], scaling the extrapolated input power by the same parameter obtained from a hydrophone (H-108, Sonic Concepts, Inc., Bothell, USA) which was calibrated at lower voltages. The compressional pressure was found to be 136.9 MPa, with the rarefactional pressure being -15.9 MPa in degassed water, which was slightly higher than the $15MPa$ threshold for generating cavitation in shock scattering [6].

The parameters provided in our study were verified using red blood cells (RBCs) embedded within an agarose hydrogel [39]. A typical histotripsy

Author Manuscript

pattern with a sharp border was observed under microscopy, and no remaining RBCs were found in the treated histotripsy region (bottom right in the Fig. S2). The temperature rise at the focus was monitored with a K-type thermocouple, which was maintained below 6℃ throughout a 15-minute histotripsy treatment (Fig. S3), distinguishing histotripsy from thermal HIFU.

The transducer was positioned in an acrylic tank filled with degassed water at room temperature. The phantom was placed in the customized acrylic container with an open side facing the transducer (Fig. 3). The focus of the transducer was aligned under B-mode US imaging guidance toward the lower portion of the specific bubble wrap compartment, to avoid any effects of residual gas remaining after cell suspension injection.

Histotripsy was applied for 30 seconds to cancer cells in suspension. The removal of the suspension mirrored the bubble wrap compartment filling procedure, with a syringe and 22-gauge needle collecting the suspension and gently injecting the suspension into a 1.5 mL EP-tube for for further processing.

Heating process

Samples from the heating-alone, and histotripsy with subsequent heating groups underwent 10-minute heating in a 50℃ [47, 35, 48] water bath (DKB-8A, Shanghai Jinghong Laboratory Instrument Co., Ltd, China). With the transient temperature curve recorded by the K-type thermocouple in this study, the CEM43 for heating was calculated to be 1429 minutes using the following equation:

$$CEM43 = \int_0^{\mathrm{t}} R^{43-T_i} dt(\mathrm{min}), where R = \begin{cases} 0.5, T_i > 43°C \\ 0.25, T_i < 43°C \end{cases} \quad (1)$$

Author Manuscript

Cell viability examination

Cell viability was assessed based on the normalized concentration of living cells post-therapy. The evaluation involved two aspects: the immediate normalized concentration of living cells after therapy and the subsequent change in the normalized concentration of residual living cells during a 96-hour culture period.

VX2 cancer cell suspensions underwent centrifugation at 445 G for 5 minutes immediately after the treatment. The supernatant was removed. For immediate examination of living cells, cells were re-suspended in 1 mL DMEM media supplemented with 100 $units/mL$ penicillin & 100 $\mu g/mL$ streptomycin. For the subsequent 96-hour culture, cells were re-suspended in DMEM media supplemented with 10% FBS, and 100 $units/mL$ penicillin & 100 $\mu g/mL$ streptomycin, at a concentration of 200,000 $living\ cells/mL$. During the culture, 5 mL of fresh media supplemented with 10% FBS, and 100 $units/mL$ penicillin & 100 $\mu g/mL$ streptomycin was added to the culture dish every day before collection for examination of cell viability. The Typan Blue Staining Cell Viability Assay Kit (catalog number C0011, Beyotime, Shanghai, China) was utilized for cell staining, following the manufacturer's instructions. Living and dead cell counts in Typan Blue-stained samples were determined using an automated cell counter (Nexcelom, cellometer Mini, USA). Additionally, the Calcein/PI Cell Viability/Cytotoxicity Assay Kit (catalog number C2015M, Beyotime, Shanghai, China) was employed to ensure the accuracy of concentrations, following the manufacturer's instructions. Samples were imaged using a fluorescence microscope (Leica DMI3000B, Buffalo Grove, IL) with emission wavelengths of 510 nm (excita-

Author Manuscript

tion frequency of 450-490 nm) and 580 nm (excitation frequency of 515-560 nm), respectively. Image analysis was performed using Fiji/ImageJ software.

The normalized concentration immediately after therapy (termed C_0^{norm}) was calculated as:

$$C_0^{\text{norm}} = \frac{N_{living,after}}{N_{living,before}} \tag{2}$$

where $N_{living,after}$ represented the number of living cells immediately after therapy, and $N_{living,before}$ was the number of living cells before therapy.

The normalized concentration of residual living cells (termed C_t^{norm}) during a 96-hour culture period was calculated as:

$$C_t^{\text{norm}} = \frac{N_{living,t}}{N_{living,t_0}} \tag{3}$$

where $N_{living,t}$ represented the number of living cells in the selected sample at time t (at 3h, 6h, 9h, 12h, 24h, 36h, 48h, 72h, and 96h during culture), and N_{living,t_0} was the number of living cells initially seeded in the culture dish.

A series of equations were linearly combined to describe the growth pattern of living cells [49]. The well-known logistic growth (LG) law model was employed to describe the normal proliferation of solid tumor cells [50]. Additionally, the linear-quadratic (LQ) model was utilized, assuming that there were two components to cell killing: a part proportional to the therapy dose and another part proportional to the square of the dose [51]. In this study, the LQ model was adapted, wherein the dose was substituted with cultured time, considering apoptosis in non-synchronized cells with different susceptibility in different phases of the cell cycle [52]. Specifically, cells in G0 or G1 phase exhibited relative resistance to apoptosis [53], while G2/M cells were more predisposed to apoptosis [54]. The final equation was expressed as:

Author Manuscript

$$y(t) = \alpha * \frac{c_0 * c_\infty}{(c_0 + (c_\infty - c_0) * e^{-k_0 * t})} + (1 - \alpha) * c_0 * e^{k_1 * t + k_2 * t^2} \quad (4)$$

note that

$$y(0) = c_0 \quad and \quad y(\infty) = \alpha * c_\infty \quad (5)$$

where α was a fitted parameter representing the fraction of cells undergoing proliferation, $\alpha * c_0$ represented initial cell population engaged in exponential proliferation, $\alpha * c_\infty$ represented the saturation cell population within finite space, $(1 - \alpha) * c_0$ represented initial cell population that underwent delayed death, $k_0 > 0$ was a fitted positive constant describing the proliferation rate, and $k_1 \leq 0$ & $k_2 \leq 0$ were fitted constants that represented the linear and quadratic components of cell killing, respectively. All the above mentioned fitted parameters for Eq. 3 were obtained with a least squares approach.

Cell proliferation examination

VX2 cancer cells were labeled with the CFDA SE Cell Proliferation Assay and Tracking Kit (catalog number C0051, Beyotime, Shanghai, China) one day before experimental procedures to assess cell division, following the manufacturer's instructions. CFDA SE was distributed approximately equally among the progeny, allowing the monitoring of cell division through successive halving of fluorescence intensity. This process was observed using a fluorescence microscope (Leica DM6 B, Buffalo Grove, IL) with an excitation filter of 480/40nm and an emission filter of 527/30nm. Fiji/ImageJ software and MATLAB (MathWorks, Natick, MA, USA) were utilized for segmenting

the living cells and calculating the average fluorescence intensity. Normalized fluorescence intensity [55] was calculated for quantitative analysis as:

$$normalized\ intensity = \frac{SI_{target}}{SI_{control}} \tag{6}$$

where SI_{target} represented the fluorescence intensity in targeted group, and $SI_{control}$ represented the fluorescence intensity in control group. The normalized fluorescence intensity was calibrated using a curve generated by the CFDA SE fluorescence intensity in the blank control group during a 3-day normal culture.

HSP70 detection

Samples from the experimental groups underwent an initial centrifugation at 300G for 5 minutes, followed by a second centrifugation at 12,000G for 10 minutes to eliminate any fragments. The supernatant was collected and stored at 4℃. Cells were lysed using RIPA Lysis Buffer (Thermo Fisher Scientific, Bremencity, Germany) at 0℃ in an ice-water mixture for 30 minutes, and the lysates were also stored at 4℃. Concentrations of intracellular and extracellular HSP70 were determined using enzyme-linked immunosorbent assay (ELISA) (catalog number FT-T509121, Shanghai FanTai Biotechnology Co., Ltd, China), following the manufacturer's instructions.

Statistical analysis

The results are presented as mean ± SD, unless otherwise specified. Statistical significance was determined using Student's t-test, with p values less than 0.05 considered statistically significant.

Author Manuscript

Author Manuscript

Results

Effect of the phantom

The phantom demonstrated stability during one-week storage at 4℃, showing no signs of dehydration upon visual inspection. Each bubble wrap compartment was filled with approximately 400 μl of DMEM media. Following histotripsy, B-mode ultrasound imaging revealed no leakage of the generated bubble clouds or deformation of the bubble wrap compartment shape. To assess potential adverse effects of the phantom, the normalized concentration of cancer cells collected from the phantom was examined as a negative control group. Representative bright field and fluorescent field images of the blank control and negative control groups are presented in Fig. 4(a) and 4(b), respectively. The fluorescent images were merged. Approximately 84.4 ± 9.3% living cells were collected after injection and retrieval from the bubble wrap compartments, demonstrating an acceptable loss compared to the 89.8 ± 5.9% in the blank control group, with no significant difference observed. Typan Blue staining yielded 85.5 ± 7.5% living cells in the negative control group and 90.0 ± 7.9% in the blank control group. No significant difference was detected between the two staining methods.

Imaging for guidance and monitoring

The B-mode images of the phantom are illustrated in Fig. 5. In Fig. 5(a), the middle layer of the phantom, containing four bubble wrap compartments, was aligned parallel to the imaging plane (xz-plane in therapy, Fig. 3), giving a cross-sectional view of the bubble wrap compartments (yz-plane in therapy, Fig. 2 and Fig. 3) in the B-mode ultrasound image before therapy. The

Author Manuscript

boundary of bubble wrap compartments produced strong reflections in the B-mode images, which helped locate the target for histotripsy. In Fig. 5(b), the phantom was horizontally rotated to the position for histotripsy, and the middle layer containing bubble wrap compartments became orthogonal to the imaging plane. The longitudinal view (xz-plane in therapy, Fig. 2 and Fig. 3) of bubble wrap compartments is visible under the B-mode ultrasound image, outlined in yellow in Fig. 5(b) and 5(c). The focal dimensions of the ultrasound field were measured as 0.47 mm in width and 3.0 mm in length (-6dB) in degassed water. The bubble cloud generated in suspension during histotripsy was observed throughout the compartment, as seen in figure 5(b) and video S1. The cavitation bubble cloud showed strong echo intensity in the B-mode image (comparing Fig. 5(b) with 5(c)). Additionally, the cavitation induced a turbulent flow encompassing the entire bubble wrap compartment (Video S1, available online) and likely VX2 cancer cells were redistributed. It was possible that a few cells might escape the histotripsy exposure. Once ultrasound field was turned off, the echogenicity of the contents in the targeted bubble wrap compartment gradually declined over the following 5 seconds.

Synergetic effects with addition of thermal therapy

A synergistic effect was observed in the immediate damage to VX2 cancer cells when histotripsy was combined with subsequent heating, as depicted in Fig. 6. The normalized concentration assessed immediately after treatment (C_0^{norm}) using Trypan Blue staining showed no significant differences among the blank control, negative control, and heating-alone groups, while treatment with histotripsy alone for 30 seconds led to a viability decrease to 18.7 $\pm$ 5.7%. When histotripsy was combined with subsequent heating, viability

Author Manuscript

furtherly dropped to 11.8 ± 3.8%, which was significantly lower than the histotripsy-alone group ($p < 0.01$).

A synergistic effect was also evident when assessing the proliferation of residual living cells after treatment, as illustrated in Fig. 7. The p-values from comparisons between each pair of groups at different time points are listed in Fig. S1. The fitted curves showing concentrations changes over time are depicted in Fig. 8, and the corresponding fitted parameters are listed in Table 1.

The normalized concentration of living cells (C_t^{norm}) in negative control and blank control groups exhibited no significant differences during the initial 24 hours of culture (Fig. 7(a)-(d)). The residual living cells exhibited exponential proliferation over time, although at different rates. By 36 hours (Fig. 7(f)), the living cells in the negative control group exhibited slower proliferation compared to the blank control group. This difference in normalized concentration continued to grow as time progressed (Fig. 7(f)-(i), Fig. 8).

In the histotripsy alone group, lower normalized concentrations (C_t^{norm}) were observed from 3 hours to 48 hours compared to either blank control or negative control group (Fig. 7(a)-(g), Fig. 8). Initially, a decreased concentration of living cells could be observed by 12 hours. After that, the residual living cells proliferated at a similar rate in the histotripsy alone group compared to the control group. By 72 hours, the normalized concentration of living cells in the histotripsy alone group reached an equivalent level to the negative control group (Fig. 7(h), Fig. 8).

In the combination of histotripsy with subsequent heating, significantly lower concentrations of living cells (C_t^{norm}) were observed compared to the

Author Manuscript

histotripsy alone group (Fig. 7, Fig. 8). In comparison to the heating alone group, histotripsy with subsequent heating consistently resulted in significantly lower concentrations from 3 hours to 96 hours. Both the fitted curves of the heating alone and histotripsy with subsequent heating groups showed continuous downward trends until reaching an extremely low level.

Bright field microscopy in Fig. 9 illustrates the appearance of residual cancer cells in the blank control, negative control, and histotripsy alone groups, which appeared fusiform with several points attached to the culture dish. In the groups treated with heating (Fig. 9(c), 9(e)), the cells maintained a round (detached) morphology throughout the 96-hour observation period. In theory, heating alone with a thermal dose of 1429 minutes should be sufficient to cause complete cell death. However, it was observed that 80.15% of the cells survived immediately after therapy (Fig. 6). During the subsequent 96-hour culture period, 26.97% of these residual cells survived to the end (Fig. 7(i), 8). According to a recent study [56], heating at 50℃ for 10 minutes might not only lead to extensive necrosis of tumor cells, but also enhance the proliferation capacity of the surviving cells by decreasing the percentage of cells in the G0/G1 phase and increasing the proportion of cells in the S phase. In our study, the fitted k_0 representing the average proliferation rate during the 96-hour culture period was 0.134 in the heating alone group, higher than 0.049, 0.047, 0.061, and 0.023 in blank control, negative control, histotripsy alone, and histotripsy with subsequent heating groups, respectively (Table 1). The lowest fitted k_0 representing average proliferation rate during the 96-hour culture period was found in the histotripsy with subsequent heating group, indicating the effectiveness of combining histotripsy and subsequent

Author Manuscript

heating.

Fluorescence observations on cell proliferation

To assess the proliferation of residual living cancer cells exposed to different therapies, we selected the 48-hour time point, noting that the first term representing proliferation on the right side of Equ. 3 was far larger than the second term representing delayed death. At that time, the normalized fluorescence intensity of CFDA SE within cells was analyzed (Fig. 10). The blank control group was regarded as the baseline for normalization. No significant differences were observed among the blank control, negative control, heating alone, and histotripsy alone groups. The degree of CFDA SE in the histotripsy with subsequent heating group was nearly 5 times that of the blank control group, 2 times that of the heating-alone group, and 3 times that of the negative control and histotripsy-alone groups after calibration, which demonstrated reduced generation of daughter cells. These findings showed that the combination of histotripsy and subsequent heating might result in synergetic effects compared to either histotripsy alone or heating alone.

Tumor-related HSP70 generation and release

To gain deeper insights into the mechanisms underlying histotripsy with subsequent heating, the HSP70 level from cancer cells was assessed (Fig. 11). In comparison to the blank control group, no significant difference was noted in the negative control group. Both heating and histotripsy led to a noticeable increase in total HSP70 levels (Fig. 11(a)), while histotripsy with subsequent heating exhibited a further elevation of HSP70. Additionally, the

Author Manuscript

intracellular (Fig. 11(b)) and extracellular (Fig. 11(c)) quantities of HSP70 were examined. Heating alone resulted in decreased intracellular HSP70 compared to the blank control group. Histotripsy with subsequent heating significantly increased the intracellular HSP70 level compared to the negative control group, whereas no significant difference was detected between the histotripsy alone group and the negative control group. Regarding extracellular HSP70, the control groups showed levels below the detection limit of ELISA. As for the experiment groups (Fig. 11(c)), heating seemed to prompt a greater release of HSP70 into the suspension. Histotripsy with subsequent heating amplified both the intracellular and extracellular HSP70. These observations contributed to the significant increase in the overall amount of HSP70 in the histotripsy with subsequent heating group.

Discussion

Histotripsy, as a minimally-invasive and non-ionizing modality, has gained considerable attention as a promising cancer treatment. A concern in its application has been whether the residual cancer cells following histotripsy might contribute to regrowth. In this *in vitro* study, it was noted that the culturing of the residual living cells resulted in proliferation equivalent to the control group when histotripsy alone was applied. The residual living cells might have escaped histotripsy successfully, which could be caused by incomplete coverage of cavitation exceeding the threshold of histotripsy. This observation aligns with findings by Worlikar et al.[18] on an immune-compromised murine model. Post complete histotripsy treatment of a tumor, demonstrated by a hypoechoic zone on ultrasound imaging, residual

Author Manuscript

cancer cells could lead to tumor regrowth, as evidenced by MRI at 3 to 9 weeks. Additionally, Hendricks-Wenger et al. [57] observed tumor regrowth in immune-compromised NSG mice, occurring in the same location as the primary tumor by the end of the 60-day study, despite receiving a full tumor ablation with a narrow margin. This was attributed to the presence of residual cancer cells. These phenomena point to the necessity of margin control in histotripsy therapy.

In this study, we demonstrate that the combination of histotripsy and controlled heating enhances immediate direct killing effects and maintains continuous suppression on proliferation. Bright field microscopy images suggest that residual cells maintain a rounded shape after exposure to heating and lack attachment to the culture dish (Fig. 9(c), 9(e)). This phenomenon might be attributed to damage to subcellular structures following heating. Luchetti et al [58] observed a deep rearrangement of actin organization during apoptosis after heating at 43℃ for 1 hour. Additionally, Pawlik et al. [59] noted changes in the microtubule network, accumulation of tubulin in the perinuclear region, and condensed and disassembled β-tubulin in shrunken and rounded H1299 lung cancer cells after heating at 43.5℃ and 45℃ for 30 minutes. In our study, such influences on subcellular structures persisted throughout the entire 4-day normal culture as evidenced by this rounded appearance.

The combination of histotripsy and subsequent heating also altered the proliferation of living cells. In a recent study, Hay et al. [60] observed a smaller population of histotripsy-ablated canine osteosarcoma cells compared to the sham-treated or untreated group, along with a decline in cell

Author Manuscript

proliferation after several divisions. In our study with VX2 cells, both heating alone and histotripsy alone trended toward decreasing cell proliferation compared to control groups, but without statistically significant differences. However, histotripsy with subsequent heating showed a significant decrease in cell proliferation compared to all other groups (Fig. 10). The decreased frequency of mitosis in proliferation contributed partly to the extremely low survival of the residual cancer cells. In our future studies, it might be worthwhile to explore the effectiveness of the histotripsy with subsequent heating on killing different types of cancer cells.

Apart from the impact on cancer cells proliferation, histotripsy with subsequent heating also affected both intracellular and extracellular HSP70 levels. The distinctive roles played by histotripsy and heating were elucidated in Figure 11. Histotripsy alone significantly increased the intracellular HSP70 compared to heating alone. Studies have shown that the expression of heat shock proteins might lead to an increased concentration of filamentous actin (F-actin) at the cell cortex during the first 24 hours after therapy, reinforcing the stability of stress fibers [61]. This phenomenon could further enhance the stability of microfilaments, bolster thermotolerance, and expedite recovery after disruptions [62, 63]. The elevated intracellular HSP70 level might confer protection against subsequent interventions during early stages. In our study, at 3 hours post-treatment, a trend of increased normalized concentration of living cells (C_t^{norm}) in the histotripsy with subsequent heating group compared to the histotripsy alone group was observed without statistically significant difference. It might be attributed to these protective mechanisms involving intracellular HSP70. Additionally, studies showed that as HSP70

Author Manuscript

translocated to the cell surface [64] and was released in an immunogenic form through either active secretion or passive release [65], the protective effect from HSP70 diminished. In our study, heating significantly increased release of HSP70, detected as extracellular HSP70, compared to histotripsy alone. From 6 hours onward, the concentration of living cells in the histotripsy with subsequent heating group was significantly lowered than that in the histotripsy alone group. Histotripsy with subsequent heating significantly altered the patterns of HSP70 release. By summing the intracellular and extracellular HSP70 levels, it was evident that histotripsy with subsequent heating resulted in a significant increase in the total HSP70 level.

Previous in vivo studies have shown that the release of damage-associated molecular patterns (DAMPs), including HSP70, calreticulin (CRT), and high-mobility group box protein 1 (HMGB1), both locally and in peripheral circulation from ablated tumor, could promote the M1 macrophage polarization and dendritic cell maturation [47]. Zhou et al. [66] also found the extracellular heat shock proteins could ultimately activate macrophages and promote TNF-α production in co-incubation. Additionally, released HSP70 from cancer cells *in vivo* has been shown to decrease immunosuppression mediated by myeloid derived suppressor cells (MDSCs) and activate a robust anti-tumor immune response [34]. In our study, histotripsy with subsequent heating also exhibited increased intracellular and extracellular HSP70 levels, suggesting a potential initiation of an immune response, as increased generation and release of HSP70 have been associated with such effects in these reported *in vivo* findings.

However, the extent to which the increased HSP70 levels induced by his-

Author Manuscript

totripsy with subsequent heating might function, potentially through binding with tumor antigens and leading to an immune response in the form of HSP–antigen complexes [67], merits further *in vivo* study. Additionally, differences in thermoresponse between cells cultured or isolated from the host to those in situ [68] might also yield discrepancies between *in vitro* and *in vivo* observations. Furthermore, the impacts of heating during histotripsy with subsequent heating on tumor blood vessels, interstitial flow, and the complex microenvironment might contribute to the complexity of the local immune response and final therapeutic effects. Therefore, a comprehensive *in vivo* study of the proposed combination of histotripsy and subsequent heating is essential in any case.

In tissue, cancer cells might exhibit greater resistance to histotripsy compared to those in suspension because of extracellular structures [69] such as the tissue matrix and adhesions. To translate the findings in this preliminary study to the *in vivo* environment, there are several considerations: firstly, the pressure of input acoustic wave may need to be increased in targeted tissue, which could vary depending on the specific tissue type [14, 70]. Acoustic droplet vaporization or the use of microbubbles might help lower the pressure threshold [71, 72]. Secondly, a precisely planned point-by-point scan is necessary to ensure complete tumor destruction. Furthermore, the dosage of both histotripsy and heating might be tissue-dependent in terms of the number of pulses per volume [43] and CEM43 [73].

These experiments suggested that histotripsy with subsequent heating could be a promising cancer treatment, inducing dysfunction in residual living cancer cells beyond the impacts of histotripsy alone. This effect might

Author Manuscript

be achieved through a combination of subcellular structural damage and the release of immunogenic HSP70. We envisage that histotripsy with subsequent heating might serve to prevent the regrowth of residual cancer cells, potentially enhancing the immune response already demonstrated in previous studies [21] when applied *in vivo*. Furthermore, the phantom with bubble wrap compartments embedded holds potential for a broader application in the investigation of ultrasound-cell interactions.

Conclusions

This study represents the first exploration of the combination of histotripsy and subsequent heating for the eradication of VX2 cancer cells in suspension. A tissue phantom with bubble wrap compartments embedded was developed to facilitate the collection and analysis of residual cancer cells following histotripsy. Both intracellular and extracellular HSP70 were examined. The synergistic effects of histotripsy with subsequent heating not only intensified the immediate lethal impact on VX2 cancer cells compared to histotripsy or heating alone, but also more effectively curtailed the proliferation of residual cancer cells. Given these compelling results, histotripsy with subsequent heating warrants further investigation in the context of *in vivo* validation.

Conflict of interest

The authors declare no competing interests.

Author Manuscript

Acknowledgements

This research was funded by National Key R&D Program of China (Grant No. 2023YFC2411402), and National Natural Science Foundation of China (Grant No. 51890892). The authors extend their gratitude to Ying Xin at the University of Michigan for contribution to exploration on possible parameters of ultrasound field for the generation of histotripsy.

AI declaration

During the preparation of this work the author(s) used ChatGPT 3.5 in order to polish the draft. After using this tool/service, the author(s) reviewed and edited the content as needed and take(s) full responsibility for the content of the publication.

Author Manuscript

References

[1] J.-p. Wu, J. Yu, J. B. Fowlkes, P. Liang, C. P. Nolsøe, Us-guided ablation of tumors–where is it used and how did we get there, Med-X 1 (1) (2023) 5.

[2] . G. ter Haar, C. Coussios, High intensity focused ultrasound: physical principles and devices, International journal of hyperthermia 23 (2) (2007) 89–104.

[3] V. S. Bachu, J. Kedda, I. Suk, J. J. Green, B. Tyler, High-intensity focused ultrasound: a review of mechanisms and clinical applications, Annals of biomedical engineering 49 (9) (2021) 1975–1991.

[4] L. Crum, J. Fowlkes, Acoustic cavitation generated by microsecond pulses of ultrasound, Nature 319 (6048) (1986) 52–54.

[5] K. B. Bader, E. Vlaisavljevich, A. D. Maxwell, For whom the bubble grows: physical principles of bubble nucleation and dynamics in histotripsy ultrasound therapy, Ultrasound in medicine & biology 45 (5) (2019) 1056–1080.

[6] Z. Xu, T. L. Hall, E. Vlaisavljevich, F. T. Lee Jr, Histotripsy: the first noninvasive, non-ionizing, non-thermal ablation technique based on ultrasound, International Journal of Hyperthermia 38 (1) (2021) 561–575.

[7] F. Winterroth, Z. Xu, T.-Y. Wang, J. E. Wilkinson, J. B. Fowlkes, W. W. Roberts, C. A. Cain, Examining and analyzing subcellular mor-

Author Manuscript

phology of renal tissue treated by histotripsy, Ultrasound in medicine & biology 37 (1) (2011) 78–86.

[8] V. A. Khokhlova, J. B. Fowlkes, W. W. Roberts, G. R. Schade, Z. Xu, T. D. Khokhlova, T. L. Hall, A. D. Maxwell, Y.-N. Wang, C. A. Cain, Histotripsy methods in mechanical disintegration of tissue: Towards clinical applications, International journal of hyperthermia 31 (2) (2015) 145–162.

[9] M. Hoogenboom, D. Eikelenboom, M. H. den Brok, A. Heerschap, J. J. FŘtterer, G. J. Adema, Mechanical high-intensity focused ultrasound destruction of soft tissue: working mechanisms and physiologic effects, Ultrasound in medicine & biology 41 (6) (2015) 1500–1517.

[10] K.-W. Lin, Y. Kim, A. D. Maxwell, T.-Y. Wang, T. L. Hall, Z. Xu, J. B. Fowlkes, C. A. Cain, Histotripsy beyond the intrinsic cavitation threshold using very short ultrasound pulses: microtripsy, IEEE transactions on ultrasonics, ferroelectrics, and frequency control 61 (2) (2014) 251–265.

[11] G. R. Schade, Y.-N. Wang, S. D'Andrea, J. H. Hwang, W. C. Liles, T. D. Khokhlova, Boiling histotripsy ablation of renal cell carcinoma in the eker rat promotes a systemic inflammatory response, Ultrasound in medicine & biology 45 (1) (2019) 137–147.

[12] V. Bollen, S. A. Hendley, J. D. Paul, A. D. Maxwell, K. J. Haworth, C. K. Holland, K. B. Bader, In vitro thrombolytic efficacy of single-and

Author Manuscript

five-cycle histotripsy pulses and rt-pa, Ultrasound in medicine & biology 46 (2) (2020) 336–349.

[13] R. J. van den Bijgaart, D. C. Eikelenboom, M. Hoogenboom, J. J. Fütterer, M. H. den Brok, G. J. Adema, Thermal and mechanical high-intensity focused ultrasound: perspectives on tumor ablation, immune effects and combination strategies, Cancer Immunology, Immunotherapy 66 (2) (2017) 247–258.

[14] E. Vlaisavljevich, Y. Kim, G. Owens, W. Roberts, C. Cain, Z. Xu, Effects of tissue mechanical properties on susceptibility to histotripsy-induced tissue damage, Physics in Medicine & Biology 59 (2) (2013) 253.

[15] L. Arnold, A. Hendricks-Wenger, S. Coutermarsh-Ott, J. Gannon, A. N. Hay, N. Dervisis, S. Klahn, I. C. Allen, J. Tuohy, E. Vlaisavljevich, Histotripsy ablation of bone tumors: Feasibility study in excised canine osteosarcoma tumors, Ultrasound in Medicine & Biology 47 (12) (2021) 3435–3446.

[16] A. Simon, F. Robinson, A. Anzivino, M. Boyer, A. Hendricks-Wenger, D. Guilliams, J. Casey, D. Grider, F. Valea, E. Vlaisavljevich, Histotripsy for the treatment of uterine leiomyomas: A feasibility study in ex vivo uterine fibroids, Ultrasound in Medicine & Biology (2022).

[17] A. Hendricks-Wenger, P. Weber, A. Simon, S. Saunier, S. Coutermarsh-Ott, D. Grider, J. Vidal-Jové, I. C. Allen, D. Luyimbazi, E. Vlaisavljevich, Histotripsy for the treatment of cholangiocarcinoma liver tumors:

Author Manuscript

In vivo feasibility and ex vivo dosimetry study, IEEE transactions on ultrasonics, ferroelectrics, and frequency control 68 (9) (2021) 2953–2964.

[18] T. Worlikar, E. Vlaisavljevich, T. Gerhardson, J. Greve, S. Wan, S. Kuruvilla, J. Lundt, K. Ives, T. Hall, T. H. Welling, et al., Histotripsy for non-invasive ablation of hepatocellular carcinoma (hcc) tumor in a subcutaneous xenograft murine model, in: 2018 40th Annual International Conference of the IEEE Engineering in Medicine and Biology Society (EMBC), IEEE, 2018, pp. 6064–6067.

[19] A. Hendricks-Wenger, P. Weber, A. Simon, S. Saunier, S. Coutermarsh-Ott, D. Grider, J. Vidal-Jove, I. C. Allen, D. Luyimbazi, E. Vlaisavljevich, Histotripsy for the treatment of cholangiocarcinoma liver tumors: In vivo feasibility and ex vivo dosimetry study, IEEE TRANSACTIONS ON ULTRASONICS FERROELECTRICS AND FREQUENCY CONTROL 68 (9) (2021) 2953–2964. doi:10.1109/TUFFC.2021.3073563.

[20] G. R. Schade, J. Keller, K. Ives, X. Cheng, T. J. Rosol, E. Keller, W. W. Roberts, Histotripsy focal ablation of implanted prostate tumor in an ace-1 canine cancer model, The Journal of urology 188 (5) (2012) 1957–1964.

[21] S. Qu, T. Worlikar, A. E. Felsted, A. Ganguly, M. V. Beems, R. Hubbard, A. L. Pepple, A. A. Kevelin, H. Garavaglia, J. Dib, et al., Non-thermal histotripsy tumor ablation promotes abscopal immune responses that enhance cancer immunotherapy, Journal for immunotherapy of cancer 8 (1) (2020).

Author Manuscript

[22] J. Vidal-Jove, X. Serres-Creixams, T. J. Ziemlewicz, J. M. Cannata, Liver histotripsy mediated abscopal effect—case report, IEEE Transactions on Ultrasonics, Ferroelectrics, and Frequency Control 68 (9) (2021) 3001–3005.

[23] K. J. Pahk, C.-H. Shin, I. Y. Bae, Y. Yang, S.-H. Kim, K. Pahk, H. Kim, S. J. Oh, Boiling histotripsy-induced partial mechanical ablation modulates tumour microenvironment by promoting immunogenic cell death of cancers, Scientific reports 9 (1) (2019) 1–12.

[24] R. J. van den Bijgaart, V. E. Mekers, F. Schuurmans, T. K. Raaijmakers, M. Wassink, A. Veltien, E. Dumont, A. Heerschap, J. J. Fütterer, G. J. Adema, Mechanical high-intensity focused ultrasound creates unique tumor debris enhancing dendritic cell-induced t cell activation, Frontiers in Immunology 13 (2022) 1038347.

[25] T. Osada, X. Jiang, Y. Zhao, M. Chen, B. C. Kreager, H. Wu, H. Kim, J. Ren, J. Snyder, P. Zhong, et al., The use of histotripsy as intratumoral immunotherapy beyond tissue ablation—the rationale for exploring the immune effects of histotripsy, International Journal of Hyperthermia 40 (1) (2023) 2263672.

[26] Q. Dai, B. Cao, S. Zhao, A. Zhang, Synergetic thermal therapy for cancer: state-of-the-art and the future, Bioengineering 9 (9) (2022) 474.

[27] J. Yang, M. Hou, W. Sun, Q. Wu, J. Xu, L. Xiong, Y. Chai, Y. Liu, M. Yu, H. Wang, et al., Sequential pdt and ptt using dual-modal single-walled carbon nanohorns synergistically promote systemic immune re-

Author Manuscript

675 sponses against tumor metastasis and relapse, Advanced Science 7 (16)
676 (2020) 2001088.

677 [28] C. Napoletano, F. Taurino, M. Biffoni, A. De Majo, G. Coscarella,
678 F. Bellati, H. Rahimi, S. Pauselli, I. Pellicciotta, J. M. Burchell, et al.,
679 Rfa strongly modulates the immune system and anti-tumor immune re-
680 sponses in metastatic liver patients, International journal of oncology
681 32 (2) (2008) 481–490.

682 [29] W. Zhou, M. Yu, X. Mao, H. Pan, X. Tang, J. Wang, N. Che, H. Xie,
683 L. Ling, Y. Zhao, et al., Landscape of the peripheral immune response
684 induced by local microwave ablation in patients with breast cancer, Ad-
685 vanced Science 9 (17) (2022) 2200033.

686 [30] J. S. Chandar, S. Bhatia, S. Ingle, M. J. M. Valdez, D. Maric,
687 D. Seetharam, J. F. Desgraves, V. Govindarajan, L. Daggubati,
688 M. Merenzon, et al., Laser interstitial thermal therapy induces robust
689 local immune response for newly diagnosed glioblastoma with long-term
690 survival and disease control, Journal of Immunotherapy 46 (9) (2023)
691 351–354.

692 [31] C. Lin, Y. Zhang, K. Zhang, Y. Zheng, L. Lu, H. Chang, H. Yang,
693 Y. Yang, Y. Wan, S. Wang, et al., Fever promotes t lymphocyte traf-
694 ficking via a thermal sensory pathway involving heat shock protein 90
695 and $\alpha 4$ integrins, Immunity 50 (1) (2019) 137–151.

696 [32] C. Lin, Z. Liu, Y. Li, J. Chen, Protocol for fever-range whole-body

Author Manuscript

hyperthermia (wbh) in mice to study febrile effect on t-cell adhesion and migration, STAR protocols 2 (3) (2021) 100720.

[33] N. Zheng, A. Xu, X. Lin, Z. Mo, X. Xie, Z. Huang, Y. Liang, Z. Cai, J. Tan, X. Shao, Whole-body hyperthermia combined with chemotherapy and intensity-modulated radiotherapy for treatment of advanced nasopharyngeal carcinoma: a retrospective study with propensity score matching, International Journal of Hyperthermia 38 (1) (2021) 1304–1312.

[34] J. Zhu, Y. Lou, P. Liu, L. X. Xu, Tumor-related hsp70 released after cryo-thermal therapy targeted innate immune initiation in the antitumor immune response, International Journal of Hyperthermia 37 (1) (2020) 843–853.

[35] P. Peng, H. Hu, P. Liu, L. X. Xu, Neoantigen-specific cd4+ t-cell response is critical for the therapeutic efficacy of cryo-thermal therapy, Journal for immunotherapy of cancer 8 (2) (2020).

[36] A. B. Couillard, A. M. Zlevor, T. J. Ziemlewicz, M. A. Kisting, E. Knott, A. E. Rossebo, J. White, M. G. Lubner, L. M. Gettle, J. L. Hinshaw, et al., A comparison of histotripsy and percutaneous cryoablation in a chronic healthy swine kidney model, Journal of Vascular and Interventional Radiology 34 (11) (2023) 1986–1996.

[37] E. Vlaisavljevich, Z. Xu, A. Arvidson, L. Jin, W. Roberts, C. Cain, Effects of thermal preconditioning on tissue susceptibility to histotripsy,

Author Manuscript

ULTRASOUND IN MEDICINE AND BIOLOGY 41 (11) (2015) 2938–2954. doi:10.1016/j.ultrasmedbio.2015.07.016.

[38] A. Parvinian, L. C. Casadaban, R. C. Gaba, Development, growth, propagation, and angiographic utilization of the rabbit vx2 model of liver cancer: a pictorial primer and "how to" guide, Diagnostic and interventional radiology 20 (4) (2014) 335.

[39] A. D. Maxwell, T.-Y. Wang, L. Yuan, A. P. Duryea, Z. Xu, C. A. Cain, A tissue phantom for visualization and measurement of ultrasound-induced cavitation damage, Ultrasound in medicine & biology 36 (12) (2010) 2132–2143.

[40] D. K. Bwambok, D. C. Christodouleas, S. A. Morin, H. Lange, S. T. Phillips, G. M. Whitesides, Adaptive use of bubble wrap for storing liquid samples and performing analytical assays, Analytical chemistry 86 (15) (2014) 7478–7485.

[41] S. Aghayan, K. Weinberg, Experimental and numerical investigation of dynamic cavitation in agarose gel as a soft tissue simulant, Mechanics of Materials 175 (2022) 104486.

[42] J. A. R. Ramírez, M. I. Gutiérrez, A. V. Hernández, C. A. N. Casares, A. R. Fernandez, L. L. Salas, Acoustic cavitation detection produced by ultrasound in an agarose-gel phantom analyzed with frequencies spectrogram, in: 2020 IEEE International Instrumentation and Measurement Technology Conference (I2MTC), IEEE, 2020, pp. 1–5.

Author Manuscript

[43] T. Worlikar, T. Hall, M. Zhang, M. Mendiratta-Lala, M. Green, C. S. Cho, Z. Xu, Insights from in vivo preclinical cancer studies with histotripsy, International Journal of Hyperthermia 41 (1) (2024) 2297650.

[44] Y. Guan, M. Lu, Y. Li, F. Liu, Y. Gao, T. Dong, M. Wan, Histotripsy produced by hundred-microsecond-long focused ultrasonic pulses: A preliminary study, Ultrasound in Medicine & Biology 42 (9) (2016) 2232–2244.

[45] Y. Xin, A. Zhang, L. X. Xu, J. B. Fowlkes, The effects on thermal lesion shape and size from bubble clouds produced by acoustic droplet vaporization, Biomedical Engineering Online 17 (1) (2018) 1–14.

[46] P. Rosnitskiy, P. Yuldashev, B. Vysokanov, V. Khokhlova, Setting boundary conditions on the khokhlov–zabolotskaya equation for modeling ultrasound fields generated by strongly focused transducers, Acoustical Physics 62 (2) (2016) 151–159.

[47] J. Zhu, Y. Zhang, A. Zhang, K. He, P. Liu, L. X. Xu, Cryo-thermal therapy elicits potent anti-tumor immunity by inducing extracellular hsp70-dependent mdsc differentiation, Scientific reports 6 (1) (2016) 27136.

[48] P. Peng, Y. Lou, J. Wang, S. Wang, P. Liu, L. X. Xu, Th1-dominant cd4+ t cells orchestrate endogenous systematic antitumor immune memory after cryo-thermal therapy, Frontiers in Immunology 13 (2022) 944115.

[49] W. C. Dewey, C. C. Ling, R. E. Meyn, Radiation-induced apoptosis:

Author Manuscript

763 relevance to radiotherapy, International Journal of Radiation Oncology*
764 Biology* Physics 33 (4) (1995) 781–796.

765 [50] K. Yamamoto, K. Hosono, H. Nakayama, A. Ito, Y. Yanagi, Experi-
766 mental data for solid tumor cells: Proliferation curves and time-changes
767 of heat shock proteins, Discrete and Continuous Dynamical Systems-S
768 5 (1) (2011) 235–244.

769 [51] J. G. Bazan, Q.-T. Le, D. Zips, Radiobiology of lung cancer, in: IASLC
770 Thoracic Oncology, Elsevier, 2018, pp. 330–336.

771 [52] W. Gorczyca, J. Gong, B. Ardelt, F. Traganos, Z. Darzynkiewicz, The
772 cell cycle related differences in susceptibility of hl-60 cells to apoptosis
773 induced by various antitumor agents, Cancer research 53 (13) (1993)
774 3186–3192.

775 [53] S. M. Quirk, R. G. Cowan, R. M. Harman, The susceptibility of gran-
776 ulosa cells to apoptosis is influenced by oestradiol and the cell cycle,
777 Journal of endocrinology 189 (3) (2006) 441–453.

778 [54] F. Gao, J. Yi, J. Q. Yuan, G. Y. Shi, X. M. Tang, The cell cycle related
779 apoptotic susceptibility to arsenic trioxide is associated with the level of
780 reactive oxygen species, Cell research 14 (1) (2004) 81–85.

781 [55] M. Linares, S. Viera, B. Crespo, V. Franco, M. G. Gómez-Lorenzo, M. B.
782 Jiménez-Díaz, Í. Angulo-Barturen, L. M. Sanz, F.-J. Gamo, Identifying
783 rapidly parasiticidal anti-malarial drugs using a simple and reliable in
784 vitro parasite viability fast assay, Malaria journal 14 (2015) 1–8.

Author Manuscript

[56] H. Fu, Y. Zeng, J. Lai, W. Lin, J. Chen, C. Xu, X. Tu, et al., Sublethal heat treatment facilitates the progression of glioma by inducing the p300-recruted β-catenin through activating the nf-κb pathway (2022).

[57] A. Hendricks-Wenger, S. Saunier, A. Simon, D. Grider, D. Luyimbazi, I. C. Allen, E. Vlaisavljevich, Histotripsy for the treatment of cholangiocarcinoma in a patient-derived xenograft mouse model, Ultrasound in Medicine & Biology 48 (2) (2022) 293–303.

[58] F. Luchetti, S. Burattini, P. Ferri, S. Papa, E. Falcieri, Actin involvement in apoptotic chromatin changes of hemopoietic cells undergoing hyperthermia, Apoptosis 7 (2002) 143–152.

[59] A. Pawlik, J. M. Nowak, D. Grzanka, L. Gackowska, J. Michalkiewicz, A. Grzanka, Hyperthermia induces cytoskeletal alterations and mitotic catastrophe in p53-deficient h1299 lung cancer cells, Acta histochemica 115 (1) (2013) 8–15.

[60] A. N. Hay, E. R. Vickers, M. Patwardhan, J. Gannon, L. Ruger, I. C. Allen, E. Vlaisavljevich, J. Tuohy, Investigating cell death responses associated with histotripsy ablation of canine osteosarcoma, International Journal of Hyperthermia 40 (1) (2023) 2279027.

[61] J. N. Lavoie, E. Hickey, L. A. Weber, J. Landry, Modulation of actin microfilament dynamics and fluid phase pinocytosis by phosphorylation of heat shock protein 27., Journal of Biological Chemistry 268 (32) (1993) 24210–24214.

Author Manuscript

[62] J. N. Lavoie, H. Lambert, E. Hickey, L. A. Weber, J. Landry, Modulation of cellular thermoresistance and actin filament stability accompanies phosphorylation-induced changes in the oligomeric structure of heat shock protein 27, Molecular and cellular biology 15 (1) (1995) 505–516.

[63] N. Mounier, A.-P. Arrigo, Actin cytoskeleton and small heat shock proteins: how do they interact?, Cell stress & chaperones 7 (2) (2002) 167.

[64] F. Zhou, D. Xing, W. R. Chen, Dynamics and mechanism of hsp70 translocation induced by photodynamic therapy treatment, Cancer Letters 264 (1) (2008) 135–144.

[65] S. S. Mambula, . S. K. Calderwood, Heat induced release of hsp70 from prostate carcinoma cells involves both active secretion and passive release from necrotic cells, International journal of hyperthermia 22 (7) (2006) 575–585.

[66] F. Zhou, D. Xing, W. R. Chen, Regulation of hsp70 on activating macrophages using pdt-induced apoptotic cells, International Journal of Cancer 125 (6) (2009) 1380–1389.

[67] A. Murshid, J. Gong, S. K. Calderwood, The role of heat shock proteins in antigen cross presentation, Frontiers in immunology 3 (2012) 63.

[68] G. F. Baronzio, E. D. Hager, G. F. Baronzio, A. Gramaglia, A. Baronzio, I. Freitas, Influence of tumor microenvironment on thermoresponse: biologic and clinical implications, Hyperthermia in cancer treatment: A primer (2006) 67–91.

Author Manuscript

[69] E. Vlaisavljevich, A. Maxwell, L. Mancia, E. Johnsen, C. Cain, Z. Xu, Visualizing the histotripsy process: Bubble cloud–cancer cell interactions in a tissue-mimicking environment, Ultrasound in medicine & biology 42 (10) (2016) 2466–2477.

[70] E. Vlaisavljevich, A. Maxwell, M. Warnez, E. Johnsen, C. A. Cain, Z. Xu, Histotripsy-induced cavitation cloud initiation thresholds in tissues of different mechanical properties, IEEE transactions on ultrasonics, ferroelectrics, and frequency control 61 (2) (2014) 341–352.

[71] E. Vlaisavljevich, O. Aydin, Y. Y. Durmaz, K.-W. Lin, B. Fowlkes, Z. Xu, M. E. ElSayed, Effects of droplet composition on nanodroplet-mediated histotripsy, Ultrasound in medicine & biology 42 (4) (2016) 931–946.

[72] E. Vlaisavljevich, Y. Y. Durmaz, A. Maxwell, M. ElSayed, Z. Xu, Nanodroplet-mediated histotripsy for image-guided targeted ultrasound cell ablation, Theranostics 3 (11) (2013) 851.

[73] P. S. Yarmolenko, E. J. Moon, C. Landon, A. Manzoor, D. W. Hochman, B. L. Viglianti, M. W. Dewhirst, Thresholds for thermal damage to normal tissues: an update, International Journal of Hyperthermia 27 (4) (2011) 320–343.

Author Manuscript

Figure Captions

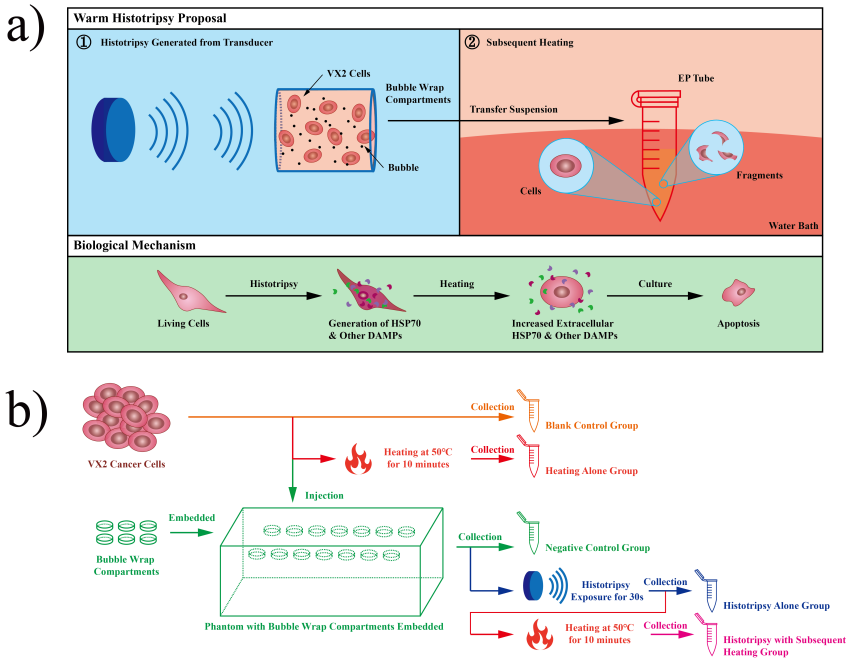

Figure 1: (a) Schematic of histotripsy with subsequent heating mechanism, intensifying immediate cellular damage, and promoting generation and release of HSP70. (b) Schematic outlining the treatments on VX2 cancer cells, where cell suspensions underwent distinct processes, including heating, histotripsy, and combined modalities.

Author Manuscript

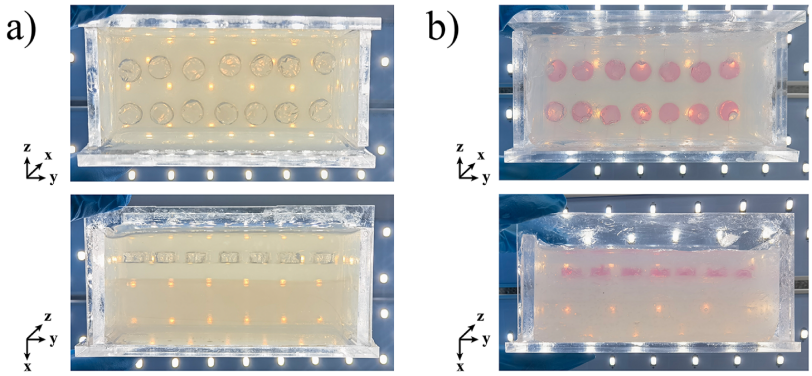

Figure 2: Photographs of the tissue phantom with bubble wrap compartments embedded in an acrylic container (a) before and (b) after injecting VX2 cancer cell suspension.

Author Manuscript

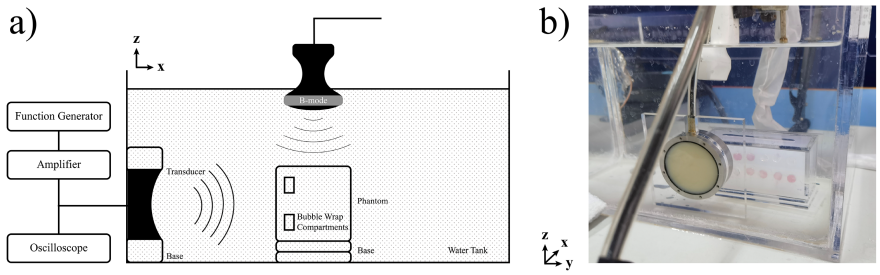

Figure 3: (a) A schematic and (b) a photograph illustrating the B-mode ultrasound imaging apparatus for guidance and monitoring of histotripsy procedure. The therapy transducer was powered by an amplifier, driven by a sine wave generated through a function/arbitrary waveform generator in burst mode. The focus was precisely aligned toward the lower portion of the specific bubble wrap compartments along z direction using a customized acrylic container and adjustment to the height of the container base. The B-mode imaging probe was securely fixed through a mechanical bracket situated at the top of the water tank.

Author Manuscript

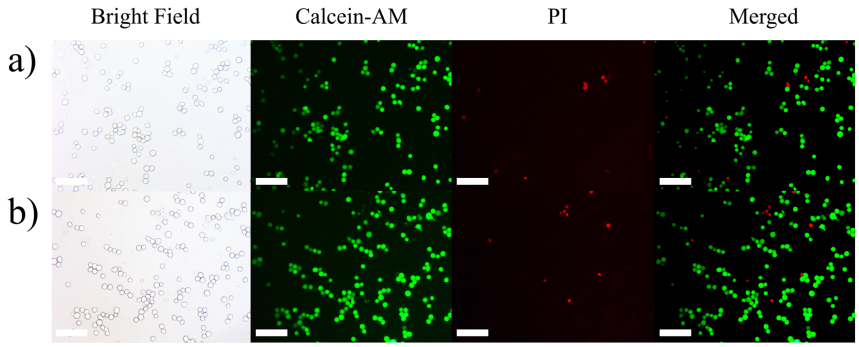

Figure 4: Representative images of the collected suspension of cancer cells from the phantom in (a) blank control and (b) negative control groups under bright field and fluorescence. Living cells are marked with Calcein-AM in green and dead cells are marked with PI in red. The fluorescent images were merged. Bar=100μm.

Author Manuscript

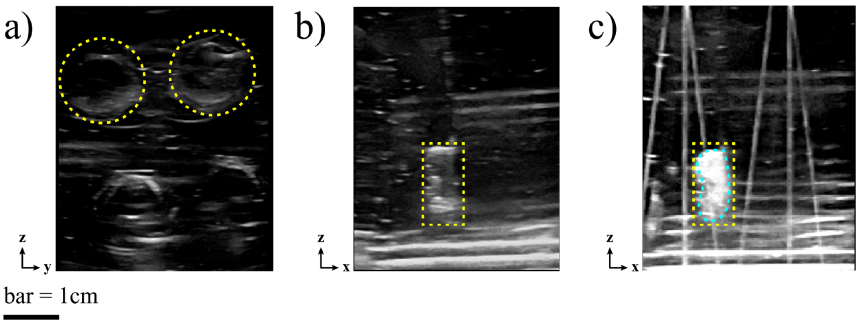

Figure 5: B-mode images of the tissue phantom with bubble wrap compartments embedded (a-b) before and (c) during the histotripsy. The imaging plane was (a) parallel or (b-c) orthogonal to the array of bubble wrap compartments. The culture media inside the bubble wrap compartments showed a low signal, similar to the water bath, while the boundary of bubble wrap compartment (yellow rectangle and ellipse) showed a stronger reflection of ultrasound. (c) A turbulent flow of bubbles (outlined in blue) inside the bubble wrap compartments was observed when histotripsy was inside the bubble wrap compartments.

Author Manuscript

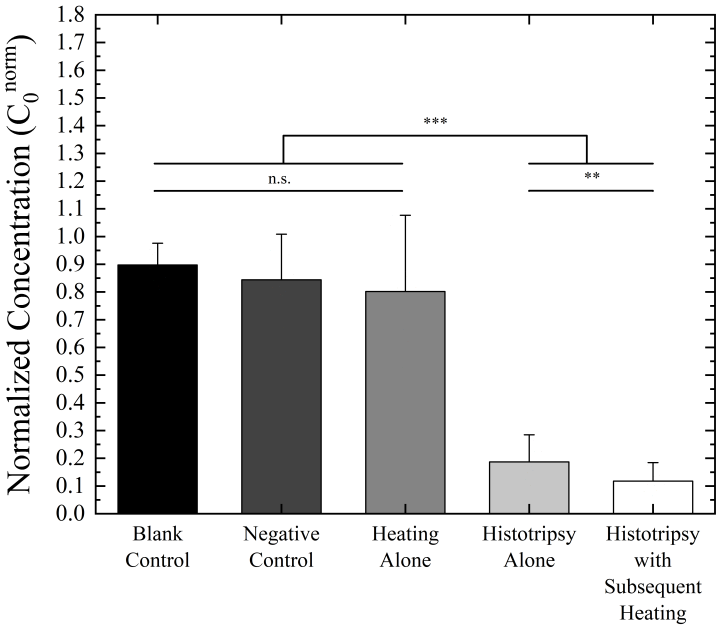

Figure 6: The normalized concentration of living cells in blank control, negative control, heating alone, histotripsy alone, and histotripsy with subsequent heating groups immediately after treatment to that before therapy.

Data are expressed as mean ± standard deviation (n = 6). *p<0.05, **p<0.01, ***p<0.001.

Author Manuscript

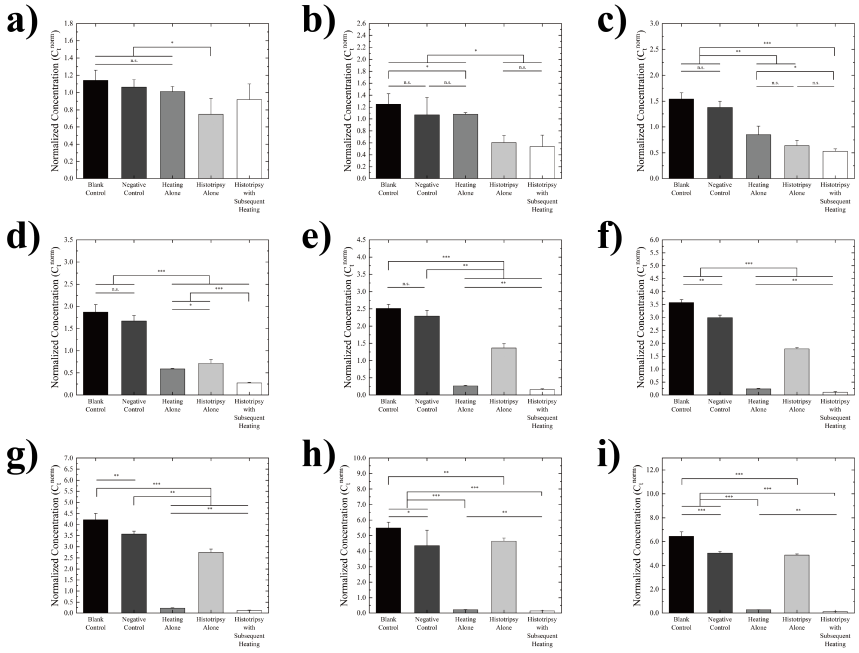

Figure 7: The change in normalized concentration of residual living cells at (a) 3h, (b) 6h, (c) 9h, (d) 12h, (e) 24h, (f) 36h, (g) 48h, (h) 72h, (i) 96h.

Data are expressed as mean ± standard deviation (n = 6). *p<0.05, **p<0.01, ***p<0.001.

Author Manuscript

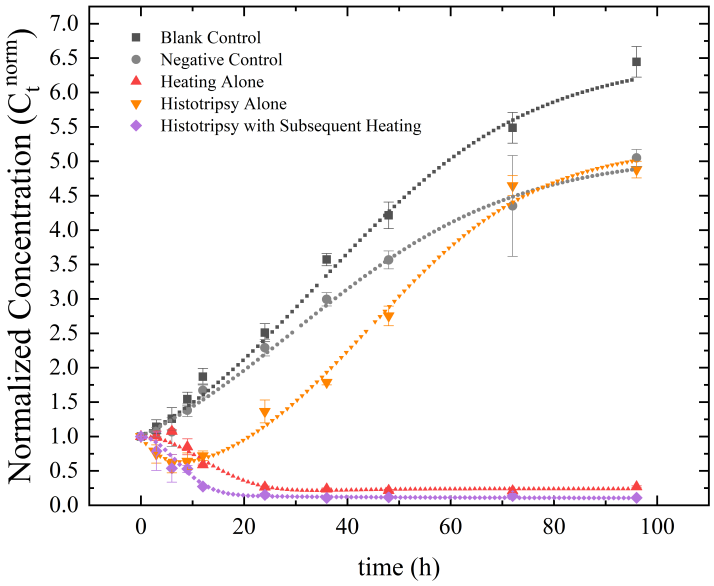

Figure 8: The fitted curves in dashed lines of normalized concentration of living cells during 96-hour continuous culture. Data are expressed as mean ± standard deviation (n = 6).

Author Manuscript

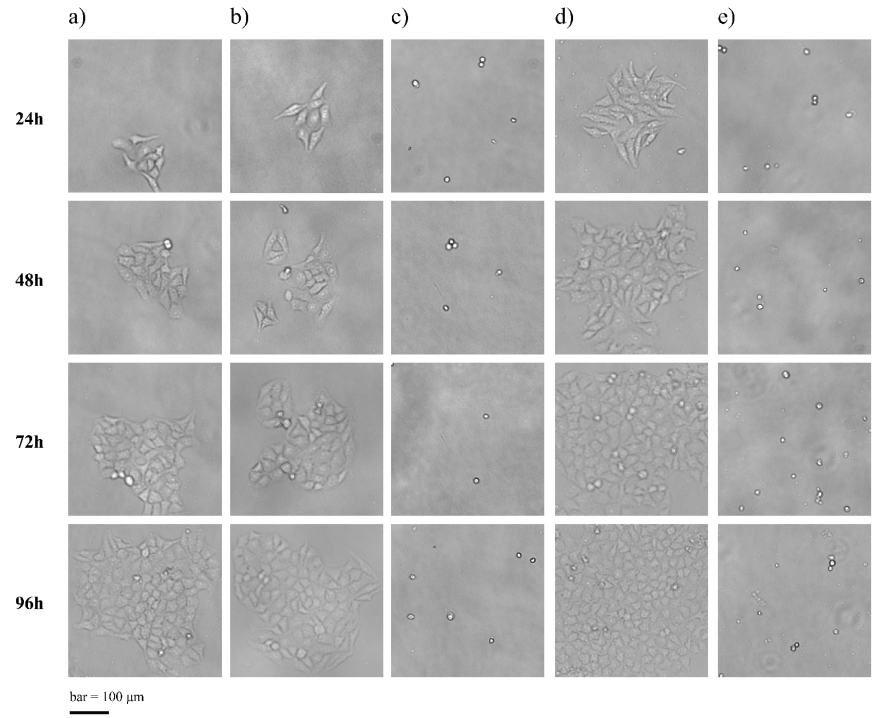

Figure 9: Representative images depicting the morphology of cancer cells in culture are presented for (a) blank control, (b) negative control, (c) heating alone, (d) histotripsy alone, and (e) histotripsy with subsequent heating groups over a time span from 24h to 96h, with equal durations organized in rows.

Author Manuscript

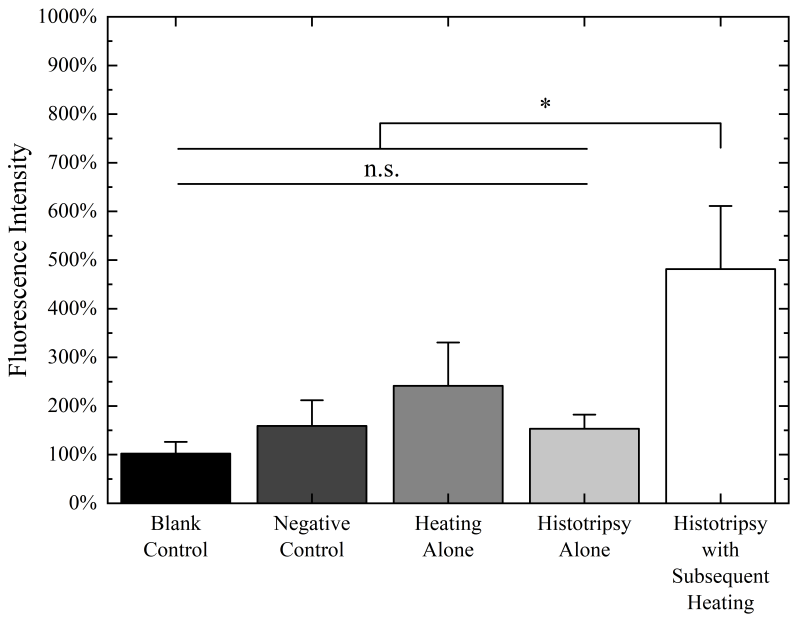

Figure 10: Normalized fluorescence intensity of CFDA SE at 48h after therapy for surviving cells following treatment for blank control, negative control, heating alone, histotripsy alone, and histotripsy with subsequent heating groups.

Data are expressed as mean ± standard deviation (n = 6). *p<0.05.

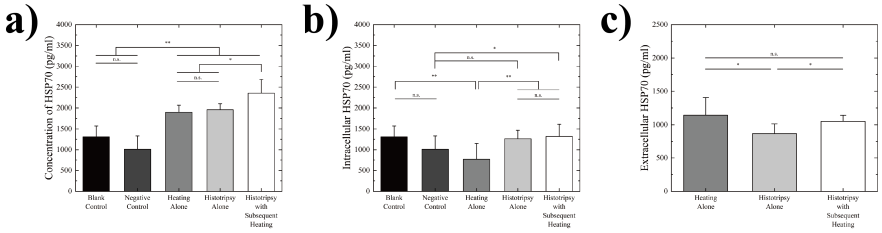

Figure 11: (a) Total amount of HSP70 generation and release in blank control, negative control, heating alone, histotripsy alone, and histotripsy with subsequent heating groups. Specifically, (b) the intracellular and (c) extracellular amount of HSP70 were compared. Note that the extracellular HSP70 control groups are not shown as their levels were below the detection limit of ELISA. Data are expressed as mean ± standard deviation (n = 6). *p<0.05, **p<0.01, ***p<0.001.

Author Manuscript

Author Manuscript

911 ## Tables

912 **Table 1:** Parameters for the Fitted Proliferation Curves of Figure 8.

913

Group	α	c_∞	$\alpha * c_\infty$	k_0	k_1	k_2	R^2
Blank Control	1.000	6.505	6.505	0.049	/	/	0.987
Negative Control	1.000	5.106	5.106	0.047	/	/	0.960
Heating Alone	0.010	23.804	0.238	0.134	0	-0.003	0.955
Histotripsy Alone	0.316	16.550	5.229	0.061	-0.201	0	0.987
histotripsy with subsequent heating	0.167	0.610	0.102	0.023	0	-0.011	0.945

914

Author Manuscript

Video Captions

Video S1: The histotripsy process on the suspension inside an air bubble revealing a turbulent flow under B-mode imaging.

Author Manuscript

Supplement Materials

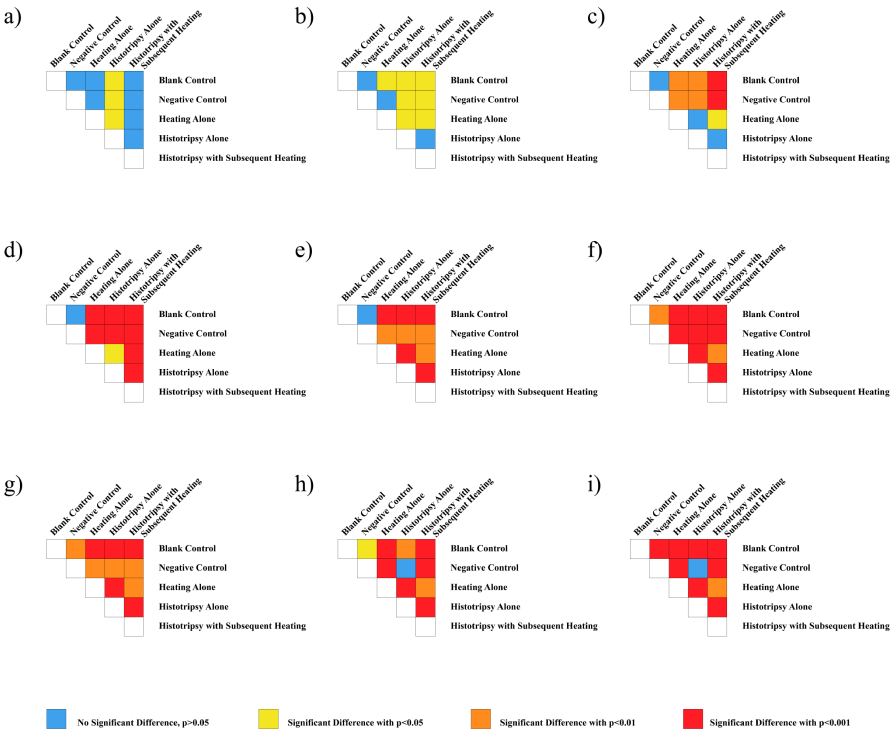

Figure S1: The p-values for the significant differences between each pair of groups for normalized concentration of living cells at (a) 3h, (b) 6h, (c) 9h, (d) 12h, (e) 24h, (f) 36h, (g) 48h, (h) 72h, (i) 96h.

Author Manuscript

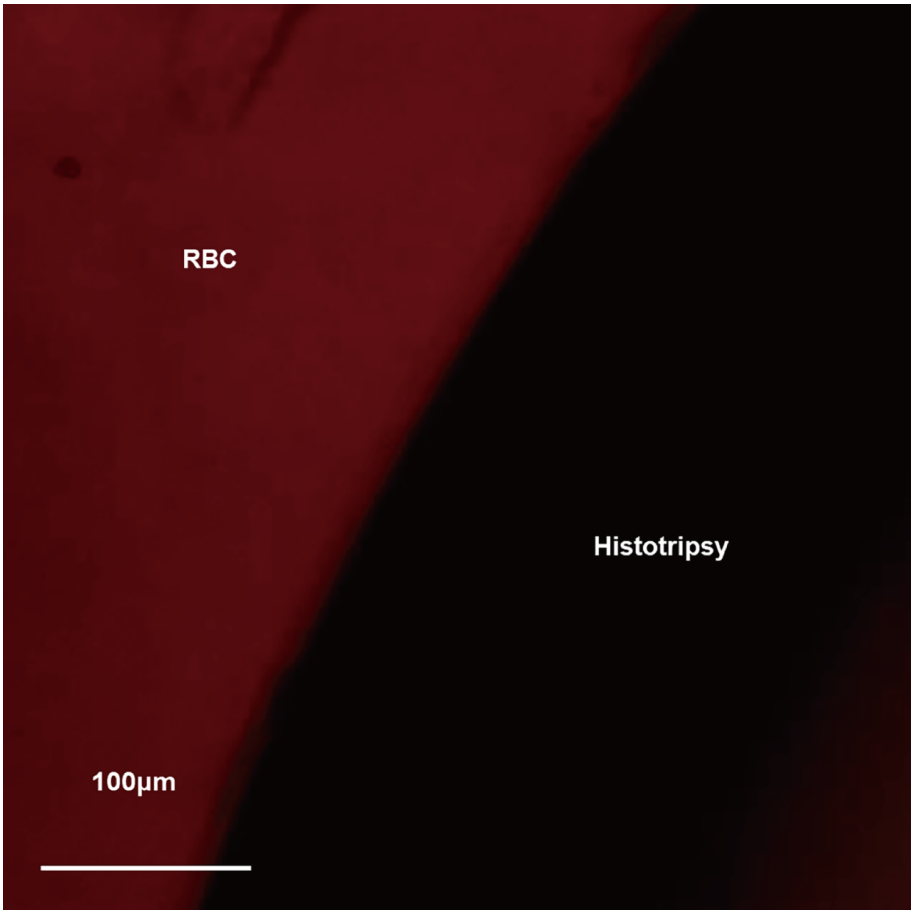

922 **Figure S2:** Microscopy micrographs of the tissue phantom after histotripsy
923 treatment at the border adjacent to the homogenized region.

Author Manuscript

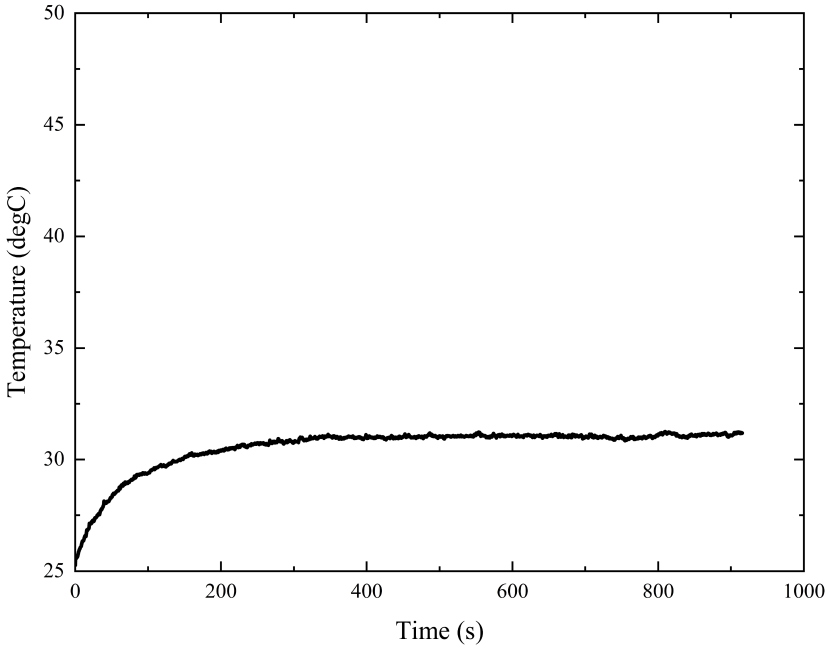

924 **Figure S3:** The temperature increase curve of histotripsy recorded with a
925 K-type thermocouple.